Electrode Reactions in DC ESR Process of Steel Rod

M. Kawakami, T. Takenaka and M. Ishikawa
Toyohashi University of Technology, Toyohashi 441-8580 JAPAN

Abstract:

The amount of non-metallic inclusion increased remarkably, when the steel rod of Fe-Ni was remelted in DC-SP mode. The silicon content increased slightly. The manganese and sulfur contents did not change. The total Al content in ingot was max. 0.7 %, while that in the electrode was 10 ppm. In DC-SP, Al^{3+} cation in slag is reduced to metallic aluminum at the slag-electrode interface, while O^{2-} anion is oxidized to $\underline{O}$ in metal pool. They are recombined to form alumina inclusion in metal pool. The amount of inclusion depended on alumina content in the slag. When the rod of plain carbon steel was remelted, however, the increment of non-metallic inclusion was as small as one tenth of that in the case of Fe-Ni rod. The amount of non-metallic inclusion did not depend on the polarity of the electrode.

1. Introduction

In 1970th, the research on electro slag remelting (ESR) process have been carried out extensively in Japan[1-10]. From then, the interest to ESR has decreased gradually. The reasons were high cost of electrical energy and the improvement of ordinary steelmaking technology which enabled the high quality steel without ESR process. One the purpose of ESR is to reduce the amount of non-metallic inclusions in steel. Recently, an attempt was made to operate a small scale DC-ESR to improve the cleanness of Fe-Ni alloy. However, the amount increased remarkably, when the steel rod of Fe-Ni was remelted in DC-SP mode.

There were some reports which showed that the total oxygen content decreased by larger scale AC ESR, if the initial value was high[7,10,11]. But in a small scale DC ESR process, it was reported that the total oxygen content increased by the process[1,2,8]. Therefore, The oxygen behavior in ESR process seems still open to question. In the DC ESR process, charge transfer reactions should occur at slag-electrode and -metal pool interfaces. The increase in the amount of inclusion is considered from electrode kinetic view point.

2. Experimentals:

The small ESR, the same as in the previous work [12], was used. The D.C. current was supplied through silicon rectifier. The capacity of the power source was 162 kVA, and the maximum D.C. current and voltage was 2.5 kA and 50 V, respectively. The electrode was driven up and down at the desired speed with the aid of electrodes driving unit. The speed was controlled manually. Figure 1 shows the schematic diagram of mold unit. The mold and stool were cooled by water. The mold was of 110 mm inner diameter and 400 mm height. Between mold and stool, the refractory ceramic matt was inserted for electric insulation. Thus, the mold was so-called insulated mold. The upper part of electrode and mold was covered with stainless steel hood which was loosely air-tight and Ar of 12 l/min(STP) was introduced to the chamber in order to prevent from air oxidation of the electrode. The electrode was of 70 mm diameter and 1300 mm length. The tip top was machined in conical shape. Two kinds of steel, Fe-Ni and plain carbon steel S25C, were used as the electrode. Their composition is shown in Table 1. The CaF_2-CaO-Al_2O_3 slag was used. The raw materials, composition of which is shown in Table 2, were blended and premelted in a graphite crucible. The slag block was crushed and stored in the hot oven.

Their composition is shown in Table 3 together with experimental operation data. In order to avoid alumina contamination of ingot, the CaF_2-CaO slag is preferable. But the slag has so high electrical conductivity that the Joule heat is apt to be insufficient. To increase the resistivity of slag, some amount of alumina was added to the slag. The amount was 1.8 kg per charge. Most of experiments were carried out in D.C. straight polarity mode(DC-SP), except when the effect of electrode polarity was examined.

The remelted ingot was cut along the central axis. The cross section was etched and observed macroscopically. The small specimen were taken from the center of ingot. They were dissolved in hydrochloric acid solution and analyzed on metallic content by induction coupled plasma (ICP) spectroscopy. The total oxygen content was analyzed by inert gas fusion IR method. Some of the pieces were dissolved completely in conc. acid mixture of nitric acid and hydrochloric acid (3 : 1), and the residue was filtered out. The amount of residue was measured and examined by EPMA to identify.

3. Results and Discussion:

3.1 Process document

Figure 2 shows an example of current and voltage change with time, where Fe-Ni rod was remelted in CaF_2-30wt%Al_2O_3 slag. The current was almost kept constant. The voltage showed periodic vibration, showing the metal droplets detachment from electrode. In the run, the average melting rate was 416 g/min. When the melting rate was large, the distance between electrode and metal pool became large, resulting in voltage increase. Since the current was constant, the voltage increase induced the increase in power supply. Thus, the distance between electrode and metal pool was kept constant by adjusting the electrode feeding rate manually. Figure 3 shows the appearance of formed ingot. The cylindrical ingot of smooth surface was obtained. All experimental operation data are shown in Table 3.

3.2 Results with Fe-Ni electrode

Table 4 shows the chemical composition of remelted ingot. The carbon, sulfur and manganese contents were the same as those of electrode. The silicon, aluminum and calcium contents were increased. The increase of aluminum content in DC ESR process has been reported by others [2,4,8]. The silicon was reduced from impurity silica in the slag as shown in Table 2. The aluminum and calcium contents depended strongly on the slag composition. The oxygen content increase remarkably compared with that in electrode, although argon hood was used to prevent air oxidation of electrode. Kojima et. al.[1,2,8] reported the oxygen increase in DC ESR of plain carbon steel regardless of electrode polarity. They suggested the possibility of electrochemical oxidation of oxygen anion in the slag. Figure 4 shows the analytical results of aluminum content in the remelted ingot at different slag composition. The horizontal axis is given by the parameter $R = X_{CaO} /(X_{CaO} + X_{Al2O3})$. Since the aluminum content in the electrode was 10 ppm, the content increased remarkably. Since the specimen was dissolved in hydrochloric acid solution, the state of aluminum was metallic aluminum. Although the content showed the maximum at R = 0.5, it decreased with R and was zero at R = 0. It can be seen that the aluminum was introduced by the reduction of alumina in the slag. Figure 5 shows the analytical results of calcium content in the remelted ingot at different slag composition. Since the solubility of calcium in molten steel is very low and CaO can easily dissolved in hydrochloric acid solution, the state of calcium might be mostly in the form of CaO. The content increased from zero to c.a. 60 ppm with R.

Figure 6 shows the amount of residue on the filter. The amount was surprisingly large. The change in the amount with slag composition was similar to that of aluminum content. Figure 7 shows the SEM image and aluminum map of residue with CaF_2-30wt%Al_2O_3 slag. The residue was of round shape and made of pure alumina which was

identified by EPMA. Figure 8 shows the SEM image and aluminum map of residue with CaF_2-30wt%CaO -10wt%Al_2O_3 slag. The residue was cubic but also made of pure alumina which was identified by EPMA. The residue obtained with CaF_2-30wt%CaO slag was not alumina but some complex oxide without alumina. The residue obtained with Al_2O_3 containing slag was made of pure alumina. This indicates that the alumina did not come from slag itself but was formed by some reactions during the remelting process. Since the process was in DC-SP mode, the cathodic reduction of alumina in the slag should occur on the electrode-slag interface. The reduced aluminum was dissolved in the metal droplets which eventually went into the metal pool. On the slag-metal pool interface, on the contrary, the anodic oxidation of oxygen anion, as well as the oxidation of dissolved aluminum, occurred to form dissolved oxygen in the pool. The dissolved oxygen and aluminum would meet each other in the pool to form alumina again. Thus, the total amount of reduced aluminum on the electrode-slag interface is the sum of dissolved aluminum and aluminum in the residue. The latter is converted from the amount of residue in Fig. 6 and shown by the open circles in Fig. 9. The total amount of reduced aluminum is shown by the closed circles in the same figure.

3.3 Results with S25C electrode

In order to examine the electrode reaction in more detail, the electrode material was change to the plain carbon steel S25C. The used slag was CaF_2-20wt%CaO-20wt%Al_2O_3. Figure 10 shows the aluminum and oxygen content in the remelted ingot. Both contents were larger than those of electrode. The results with Fe-Ni electrode were also shown for comparison. The aluminum content in S25C ingot was smaller than that in Fe-Ni. Figure 11 shows the amount of residue. The amount was very small in the case of S25C, compared with that in the case of Fe-Ni. The total amount of reduced aluminum was estimated in the same way as above and shown also in Fig. 11. The amount was on tenth of that in Fe-Ni electrode.

3.4 The effect of polarity

The effect of electrode polarity was examined using S25C electrode with CaF_2-20wt%CaO-20wt%Al_2O_3 slag. Although the average current and voltage was nearly the same in both polarity, the voltage vibration was more violent in DC-RP(reverse polarity) than in DC-SP. Thus, the operation was less stable. The melting rate, however, was larger in DC-RP than in DC-SP. This is due to the fact that the local heat generation near the electrode tip is more in DC-RP than in DC-SP, as pointed out by Kojima et. al.[1,8]. The aluminum and oxygen content were compared in Fig. 12. Both contents were slightly lager in DC-RP than in DC-SP. On the contrary, the amount of residue was smaller DC-RP than in DC-SP as shown in Fig. 13. Then, the total amount of reduced aluminum estimated in the same way as above was the same in both polarities as shown also in Fig. 13.

3.5 Reaction mechanism

Figure 14 shows the schematic diagram of reaction mechanism in the DC-SP polarity with Fe-Ni electrode. In this case, the electrode acts as cathode. Thus, the cathodic reduction of cations in the slag should occur at the electrode-slag interface. Namely,

$$Ca^{2+} + 2\,e = \underline{Ca} \quad (1)$$

$$Al^{3+} + 3\,e = \underline{Al} \quad (2)$$

$$Si^{4+} + 4\,e = \underline{Si} \quad (3)$$

$$Mn^{4+} + 4\,e = \underline{Mn} \quad (4)$$

$$Fe^{3+} + 3\,e = Fe \quad (5)$$

From the view point of oxide stability, the possibility of reaction is larger from the last one.

Since the contents of Mn^{4+} and Fe^{3+} in the slag was very small, however, the reactions of (4) and (5) might be negligible. The reaction of (3) was proved to occur, because the silicon content in the ingot was always larger than in electrode as shown in Table 4. The reaction (2) might prevail over the reaction (1), taking into account of their oxide stability. Thus, the reaction (2) is dominant as far as the alumina exists in the slag. The rate controlling step should be the electron supply, because the amount of cations near the interface was large enough. All metallic elements so-formed were dissolved in the metal droplets and eventually absorbed in the metal pool.

At the slag-metal pool interface, on the contrary, all above reactions should proceed in reverse direction. In this case, however, the rate controlling step of the reverse reaction from (1) to (4) should be the mass transfer of metallic elements in the metal pool, because the contents of these element were small. To supplement the current supply, the oxidation of oxygen anion should occur. Namely,

$$O^{2-} = \underline{O} + 2\,e \qquad (6)$$

The formed atomic oxygen should be dissolved in the metal pool, where it would react with dissolved aluminum to form alumina. The silicon would not react with the oxygen, as far as the aluminum content was large enough. This is the reason why the amount of dissolved aluminum and alumina increased in the ingot. Namely, This is attributable to the non-symmetric electrode reactions at the electrode-slag and slag-metal pool interfaces.

The fraction of current used for reduction of aluminum to the total aluminum content can be defined as the apparent current efficiency. It is shown in Fig. 15. The vales ranged from 15 to 30 % up to R = 0.5. These values do not seem unrealistic to support the above reaction mechanism.

As shown in Fig. 9, the total aluminum content had the maximum at R = 0.5. The total aluminum content would depend on the melting speed. Since the average current was almost constant, the reduction rate of aluminum would be constant regardless of slag composition. The melting rate, however, was higher with the slag of higher alumina content, as shown in Table 3. This is due to higher electrical resistance. If the melting rate was high, the reduced aluminum would be diluted by the larger amount of metal droplets to lower content. This might be one of the reasons for the appearance of maximum.

The reason why the aluminum content in Fe-Ni ingot was much higher than in S25C could be explained as follows. One reason is that the activity of aluminum in Fe-Ni should be more negatively deviated. Nickel and aluminum is well known to form intermetallic compound. Thus, it might be acceptable that the nickel should lower the activity of aluminum, although no data could be found. The other is that alumina formation and floatation in the metal pool should be accelerated by CO gas formation at the slag-metal pool interface. The carbon content in S25C was much higher than in Fe-Ni. Thus, the oxygen formed by the reaction (6) would react with the dissolved carbon to form CO bubbles.

In DC-RP mode, the anodic reaction should occur at the electrode-slag interface. Namely, the reverse reactions of (3) to (5) and the reaction (6) should occur. Those of (1) and (2) was negligible, because the aluminum and calcium content was negligibly small. In would be stricter that the reaction should occur at the slag-thin metal film interface. The amount of silicon, manganese and carbon which could be oxidized was very limited. Thus, The predominant reaction would be the reaction (6). If the oxygen content exceeded the solubility limit, the oxygen would form FeO which would be dissolved in the slag. At the slag-metal pool interface, however, all cathodic reaction of (1) to (5) should proceed simultaneously. Thus, the aluminum content in DC-RP was higher than in DC-SP as shown in Fig. 12, the amount of residue in DC-RP was smaller than in DC-SP and the total aluminum content was same in both polarity as shown in Fig. 13.

The oxidation of nickel was not observed. This is because nickel is the most stable

metallic element.

4. Concluding remarks

In DC-SP of Fe-Ni, the aluminum, silicon and calcium contents increased. The content depended on the slag composition. The increase in calcium content was not so much, because the solubility of calcium in molten steel is very limited. The total oxygen content also increased. In DC ESR of plain carbon steel, the aluminum and oxygen contents increased. But they were much smaller than those in Fe-Ni. These phenomena can be explained electrochemically by the non-symmetric electrode reactions at the electrode-slag and slag-metal pool interfaces. Thus, it is concluded that, the increase in aluminum and oxygen contents cannot be prevented in DC ESR process.

References

1. M. Inouye, Y. Kojima and M. Kato: Tetsu-to-Hagane: vol. 61(1975), pp. 139-56.
2. Y. Kojima, M. Kato, T. Toyota and M. Inouye: vol.(1975), pp.2001-11.
3. K. Ogino and S. Hara: Tetsu-to-Hagane, vol.63(1977), pp.2141-51.
4. Y. Oguti, Y. Tanbe, S. Miyama and A. Ejima: ibid., pp.2152-61.
5. M. Kawakami, K. Nagata, M. Murayama,N. Sakata, Y. Miyasita and K. Goto: ibid., pp.2161-71.
6. N. Tokumitsu, K. Harashima and Y. Nakamura: ibid., pp.2172-80.
7. A. Masui, Y. Sasajima, N. Sakata and M. Yamamura: ibid., pp.2181-90.
8. Y. Kojima, M. Kato, S. Nomura and M. Inouye: ibid., pp.2191-97.
9. S. Sawa, S. Shibuya and S. Kinbara: ibid, pp.2198-2207.
10. Y. Hirose, K. Okkohira, T. Shimizu, N. Sato, M. Hirai and M. Nishwaki: ibid., pp.2208-23.
11. K. Narita: ibid., pp.1996-2009.
12. M. Kawakami, M. Ooishi, T. Takenaka and T. Suzuki: Proc. 5th International Conference on Molten Slag, Fluxes and Salts, Sydney, (1997), pp. 477-82.

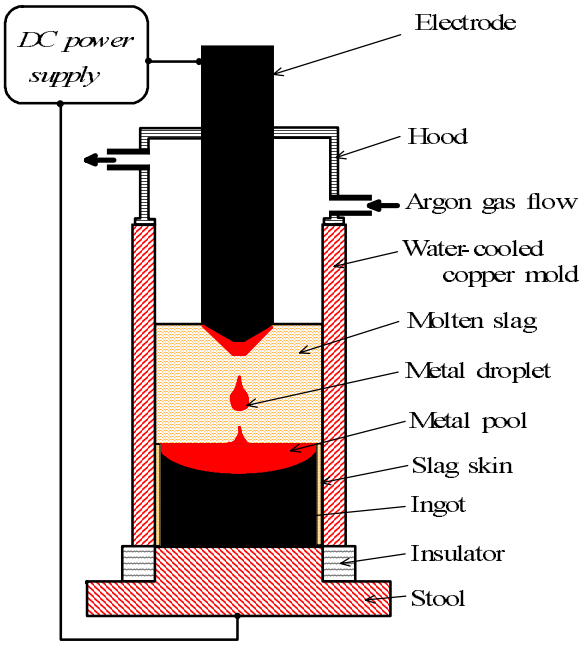

Fig.1 Schematic diagram of mold unit.

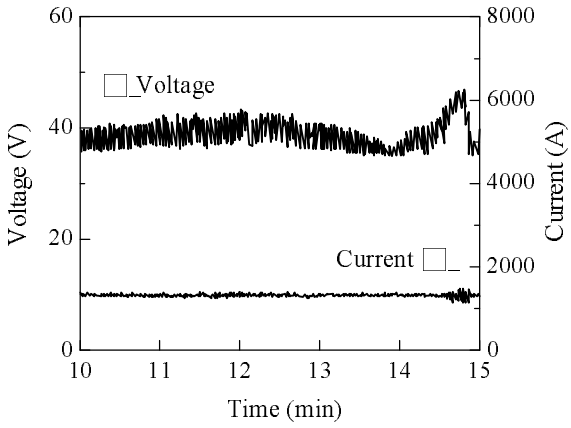

Fig.2 Changes in voltage and current with time(No.15:CaF_2-30wt%Al_2O_3, Fe-36%Ni,DCSP).

Fig.3 Appearance of ingot(No.15:Fe-36%Ni, in DCSP,CaF_2-30wt%Al_2O_3).

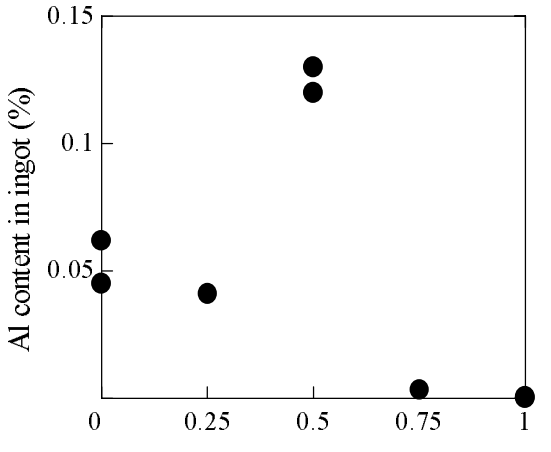

Fig.4 Dependence of aluminum content on ratio R.

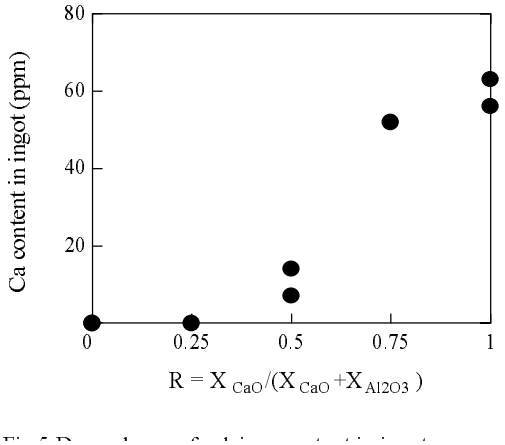

Fig.5 Dependence of calcium content in ingot on ratio R.

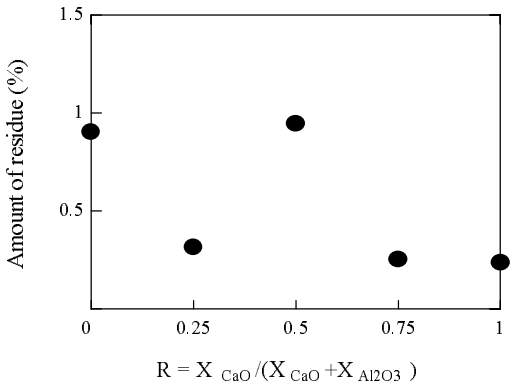

Fig.6 Dependence of amount of residue on ratio R.

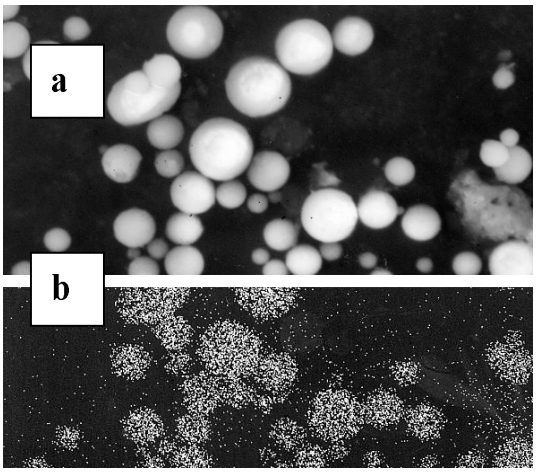

1 μ m

a: SEM image b: aluminum map

Fig.7 SEM image of residue(No.15:Fe-36%Ni,DCSP,CaF_2-30wt%Al_2O_3).

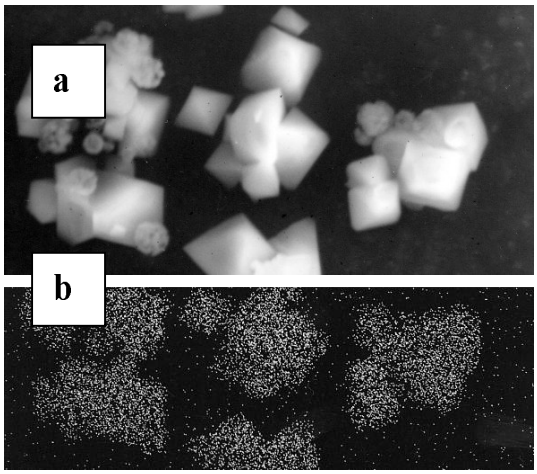

1 μ m

a: SEM image b: aluminum map

Fig.8 SEM image of residue(No.15:Fe-36%Ni,DCSP,CaF_2-30wt%CaO 10wt%Al_2O_3).

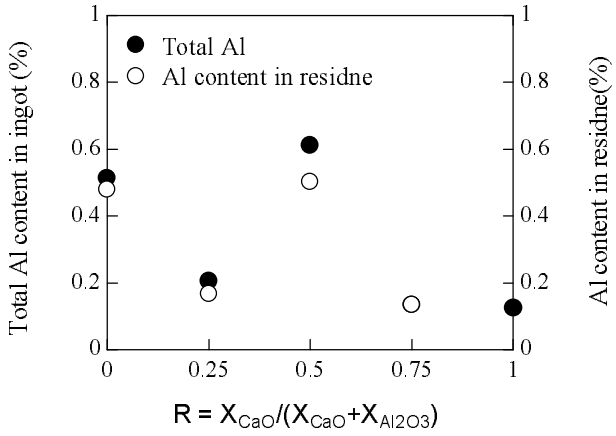

Fig.9 Dependence of total aluminum content in ingot on ratio R.

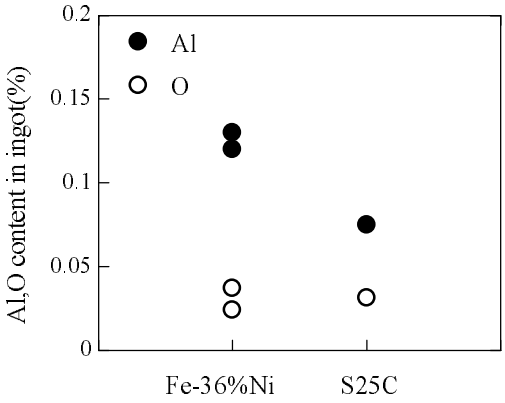

Fig.10 Aluminum and oxygen content in Fe-Ni and S25C ingots.

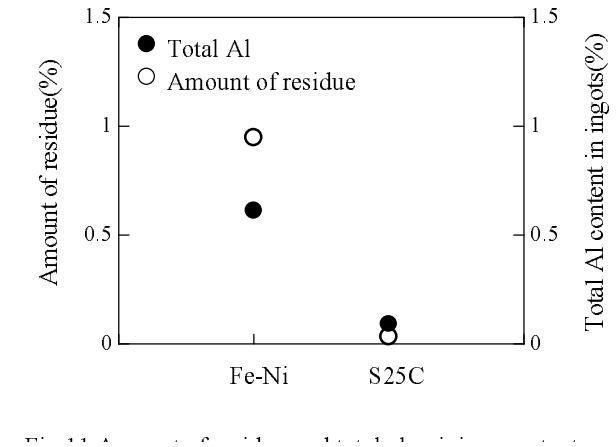

Fig.11 Amount of residue and total aluminum content in Fe-Ni and S25C ingots.

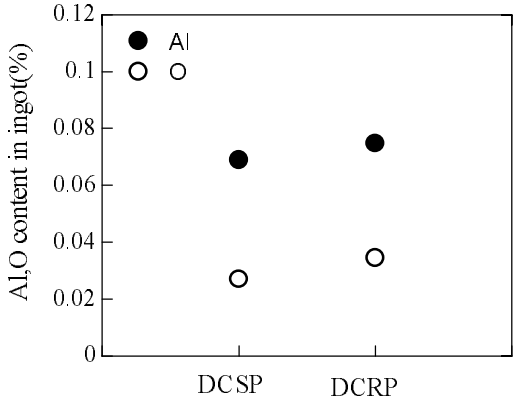

Fig.12 Aluminum and oxygen in ingot in different electrode polarity.

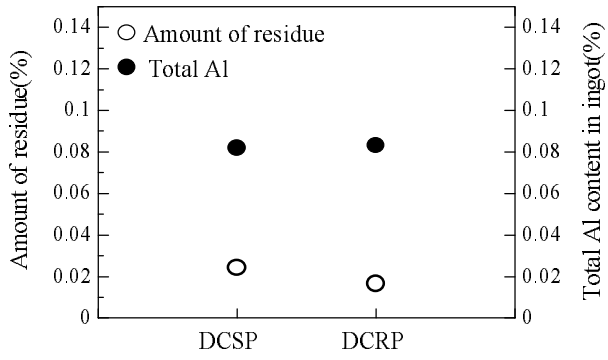

Fig. 13 Amount of residue and total aluminum content in ingot in different electrode polarity.

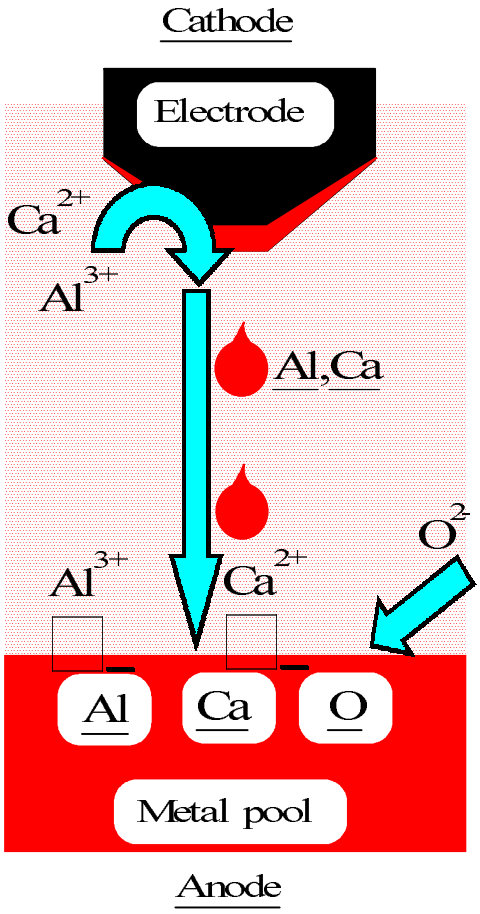

Fig. 14 Schematic diagram of reaction mechanism in DCSP.

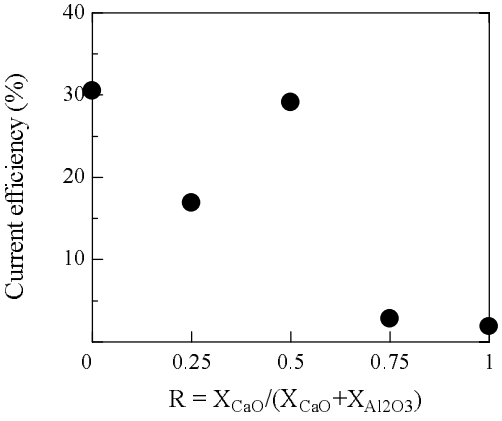

Fig. 15 Dependence of current efficiency on R.

Table 1 Chemical composition of electrode:ppm(wt%).

	C	Si	Mn	P	S	O	N	Al	Mg	Ca	Ni
Fe-Ni	32	37	(0.29)	10	13	76	4	< 10	< 10	< 10	(36.3)
S25C	(0.25)	(0.19)	(0.47)	240	60	50	20	190	-	-	(0.01)

Table 2 Composition of raw materials.

	Content (wt%)					
	CaF_2	CaO	Al_2O_3	Fe	Si	Mn
ANF-6	70	0	30	0.006	0.11	<0.001
ANF-8	60	20	20	0.084	0.19	0.035
CaF_2	100	-	-	0.017	0.43	<0.001
CaO	-	100	-	0.012	0.13	<0.001
Al_2O_3	-	-	100	0.005	0.005	<0.001

Table 3 Experimental operation data.

Run	Electrode	Slag composition				Operation condition		
		CaF_2 (wt%)	CaO (wt%)	Al_2O_3 (wt%)	R	M.R. (g/min)	i_{av} (A)	E_{av} (V)
14	Fe-Ni	60	20	20	0.5	291	1338	24
21	Fe-Ni	60	20	20	0.5	292	1344	25
33	S25C	60	20	20	0.5	203	1381	28
38	S25C	60	20	20	0.5	180	1320	28
35*	S25C	60	20	20	0.5	292	1356	29
15	Fe-Ni	70	0	30	0	416	1394	27
23	Fe-Ni	70	0	30	0	298	1200	23
16	Fe-Ni	80	20	0	1	117	1430	20
26	Fe-Ni	80	20	0	1	117	1403	21
17	Fe-Ni	60	10	30	0.25	500	1335	30
25	Fe-Ni	60	30	10	0.75	153	1385	23

M.R. : average meting rate i_{av} : average current E_{av} : average voltage

* :D.C.reverse polarity

Table 4 Chemical composition of ingot(electrode:Fe-36%Ni,polarity:DCSP).

Run	C (%)	Al (%)	S (%)	Si (ppm)	Mn (%)	Ca (ppm)	O (%)
14	0.004	0.12	0.001	66	0.24	7	0.024
21	0.003	0.13	0.002	81	0.23	14	0.037
15	0.003	0.045	0.001	64	0.21	<1	0.03
23	0.004	0.062	0.002	85	0.2	<1	0.031
16	0.003	10ppm	0.002	66	0.27	63	0.042
26	0.004	6ppm	0.001	45	0.21	56	0.039
17	0.003	0.041	0.002	49	0.18	<1	0.035
25	0.003	34ppm	0.001	30	0.21	52	0.041